HHS Public Access

Author manuscript

Mol Microbiol. Author manuscript; available in PMC 2015 June 08.

Published in final edited form as:

Mol Microbiol. 2014 September ; 93(5): 883–896. doi:10.1111/mmi.12703.

De novo morphogenesis in L-forms via geometric control of cell growth

Gabriel Billings[1], **Nikolay Ouzounov**[2], **Tristan Ursell**[3], **Samantha M. Desmarais**[3], **Joshua Shaevitz**[4,5], **Zemer Gitai**[2,**], and **Kerwyn Casey Huang**[3,6,*]

[1]Department of Physics, Stanford University, Stanford, CA 94305, USA

[2]Department of Molecular Biology, Princeton University, Princeton, NJ 08544, USA

[3]Department of Bioengineering, Stanford University, Stanford, CA 94305, USA

[4]Department of Physics, Princeton University, Princeton, NJ 08544, USA

[5]Lewis-Sigler Institute for Integrative Genomics, Princeton University, Princeton, NJ 08544, USA

[6]Department of Microbiology and Immunology, Stanford University School of Medicine, Stanford, CA 94305, USA

Summary

In virtually all bacteria, the cell wall is crucial for mechanical integrity and for determining cell shape. *Escherichia coli's* rod-like shape is maintained via the spatiotemporal patterning of cell-wall synthesis by the actin homologue MreB. Here, we transiently inhibited cell-wall synthesis in *E. coli* to generate cell-wall-deficient, spherical L-forms, and found that they robustly reverted to a rod-like shape within several generations after inhibition cessation. The chemical composition of the cell wall remained essentially unchanged during this process, as indicated by liquid chromatography. Throughout reversion, MreB localized to inwardly curved regions of the cell, and fluorescent cell wall labelling revealed that MreB targets synthesistothose regions. When exposed to the MreB inhibitor A22, reverting cells regrew a cell wall but failed to recover a rod-like shape. Our results suggest that MreB provides the geometric measure that allows *E. coli* to actively establish and regulate its morphology.

Introduction

Most bacteria adopt well-defined cell shapes and maintain those shapes during growth and across different environments (Young, 2006). In virtually all bacterial species, the peptidoglycan cell wall is a rigid, load-bearing structure that defines cell shape by balancing the mechanical stress due to turgor pressure (Holtje, 1998). Insertion of new material into the cell wall is vital to the growth of the cell, and the spatiotemporal regulation of this

*For correspondence. kchuang@stanford.edu; Tel. (+1) 650 721 2483; Fax (+1) 650 724 1922. **For correspondence. zgitai@princeton.edu; Tel. (+1) 609 258 9420; Fax (+1) 609 258 4575.

Supporting information

Additional supporting information may be found in the online version of this article at the publisher's web-site.

insertion determines both the growth and morphology of the cell. Thus, cell-wall synthesis in bacteria serves as a powerful model system for studying spatial control of enzymatic activity: there must be cellular components that can detect and respond to the shape of the cell, and control cell-wall synthesis accordingly. Although many of the enzymes responsible for synthesizing new peptidoglycan and incorporating it into the cell wall are known (Scheffers and Pinho, 2005), how this incorporation is regulated to give rise to the uniform morphology and robust growth of most bacteria is still an outstanding challenge.

Despite its key importance for bacterial physiology, the cell wall is conditionally dispensable. Many bacterial species can survive and propagate without a cell wall as 'L-forms'(Klieneberger, 1935), eitherasnaturally occurring variants of normally walled species (e.g. *Vibrio cholerae* and *Borrelia burdorferi*) (Onwuamaegbu *et al*., 2005), or generated via an external stress (Pierce, 1942). Lacking the cell wall as a rigid structure, L-forms adopt a spherical morphology consistent with inflation by osmotic pressure. Due to the absence of the load-bearing cell wall, L-form growth generally requires high-osmolarity media to reduce turgor pressure (Onoda *et al*., 1987). For experimental studies, L-forms can typically be generated either by disrupting the cell wall with drugs such as beta-lactam antibiotics, or by genetic inhibition of the cell-wall synthesis pathway (Leaver *et al*., 2009). In many L-forms, disruption of the cell wall is reversible: cells are able to regrow their cell wall and revert to their ordinary morphology once the block on cell-wall synthesis is removed (Lederberg, 1956; Onoda *et al*., 1987; Leaver *et al*., 2009). Studying the reversion process thus allows the disentangling of the action of cell-wall synthesis enzymes from their interaction with existing cell wall; during the early stages of reversion, interactions with existing cell wall can likely be neglected, facilitating the investigation of *de novo* cell-wall synthesis and providing a powerful tool to study how cell shape is programmed in bacteria.

For some variants or species of L-forms, only a very small fraction of cells revert to their normal shape, making it challenging to visualize the reversion process in individual cells (Dominguez-Cuevas *et al*., 2012). The reversion process has been studied in other cell-wall deficient bacteria such as penicillin-induced protoplasts (Lederberg, 1956) and lysozyme-induced spheroplasts (Ranjit and Young, 2013). However, neither of these systems was capable of propagating and dividing in a cell wall-free state, and in neither system were the molecular mechanisms of shape regulation elucidated. A system that facilitates the study of L-form generation, propagation, and reversion, ideally in the same cell lineage, would shed light on the mechanisms of cell-wall synthesis and morphogenesis in a system lacking initial cues from a preexisting wall.

Across bacteria, fungi, and plants, a general picture of rod morphogenesis has emerged in which cell-wall insertion is coordinated by the cortical cytoskeleton (Huang *et al*., 2012). In rod-shaped bacteria such as *Escherichia coli* and *Bacillus subtilis*, the cytoskeletal protein MreB (Gitai *et al*., 2004), a homologue of eukaryotic actin, is required for maintaining a rod-like shape. In *E. coli*, depletion of MreB or inhibition of its polymerization using the small molecule A22 causes cells to round and eventually lyse (Shih *et al*., 2005; Furchtgott *et al*., 2011). MreB moves circumferentially in a manner dependent on cellwall synthesis (Dominguez-Escobar *et al*., 2011; Garner *et al*., 2011; van Teeffelen *et al*., 2011), suggesting that MreB localization may be correlated with wall growth; indeed, we have

observed previously that MreB is associated with newly synthesized cell wall (Ursell *et al*., 2014). Moreover, recovery of *Caulobacter crescentus* cells after treatment with A22 suggested that MreB can drive the transition from a spherical to a rod-like shape (Takacs *et al*., 2010). However, neither the role of MreB in the *de novo* generation of a cell wall with a specific shape during L-form reversion nor the mechanism of shape regulation by MreB has been explored.

Here, we use quantitative imaging to investigate the reversion of *E. coli* L-forms, revealing that the MreB cytoskeleton responds to geometric cues in order to coordinate the spatial pattern of cell-wall synthesis. We describe the generation of *E. coli* L-forms by treatment with antibiotics and quantify the dynamics of their reversion to a rod-like form at both morphological and biochemical levels. The computational methods developed here facilitate detailed tracking of extremely diverse cell morphologies over time, allowing us to link localization of key cellular elements to changes in cell geometry. We demonstrate that reversion to rod-like shapes requires MreB, which localizesto regions of negative curvature and promotes the synthesis of new cell-wall material at those locations. Thus, the same machinery that is responsible for the maintenance and propagation of a rod-like morphology is also capable of establishing the rod-like shape *de novo*. Overall, our work shows that cytoskeletal-mediated control of cell-wall synthesis constitutes a robust programme for *de novo* initiation of rod morphogenesis in bacteria.

Results

E. coli L-forms revert to a rod-like shape upon removal of cell-wall inhibition

We generated L-forms of *E. coli* MG1655 using the betalactam antibiotic cefsulodin to inhibit PBP1A/B-mediated lateral cell-wall synthesis (Noguchi *et al*., 1979; Joseleau-Petit *et al*., 2007). To observe the resulting shape changes during growth in the presence of cefsulodin, we grew cells in a microfluidic chamber with L-form lysogeny broth (LFLB) (*Experimental procedures*). As expected, bleb-like bulges formed through defects in the cell wall (Fig. 1, Movie S1) (Goodell *et al*., 1976; Huang *et al*., 2008). Although some cell lysis followed these bulging events, the high osmolarity of the growth medium prevented lysis in a reasonable fraction of the cells, allowing us to observe the conversion process from rod-shaped cells to L-forms. Over time, these bulges grew and eventually separated from the rest of the cell. These roughly spherical cells, which we will refer to as L-forms, continued to propagate through growth and division.

This microfluidic platform also allowed us to wash cefsulodin out of the growth medium and to determine the process by which the propagating L-forms could revert to a walled state with a well-defined morphology, as was observed in the classic Lederberg experiments (Lederberg, 1956). Within 1 h of cefsulodin removal, the L-forms adopted non-spherical and elongated shapes indicative of cell-wall growth (Fig. 1, purple inset) and reestablished rod-shaped morphologies within a few generations (Fig. 1, blue inset). This cycle from rod-shaped to L-form and back to rod-shaped required less than 9 h for approximately 15% of cells. This rapid transition from amorphous, propagating L-forms to rod-like cells suggests that wild-type morphology is strongly programmed by the cell-wall synthesis machinery and is not simply a weak attractor (i.e. a shape that cells slowly converge to) propagated and

maintained through growth. The high frequencies and short timescales with which wild-type cells converted to L-forms and with which L-forms reverted to rod-shaped cells suggest that no specific genetic mutations are required for *E. coli* L-form generation, propagation, or reversion.

Morphological dynamics of reversion reveal that MreB is required for *de novo* rod morphogenesis

In order to investigate the reversion process in more detail, and in the absence of the mechanical constraints created by the microfluidic device, we washed an overnight culture of L-forms and placed them onto agarose pads lacking cefsulodin. We observed a similarly rapid reestablishment of rod-like morphologies (Fig. 2A, Movie S2). Initially, many of these L-forms appeared circular in the image focal plane. To determine whether the agarose pad and/or coverslip altered cell geometries, we acquired *z*-stacks of L-forms stained with the membrane dye FM4–64 (*Experimental procedures*). Deconvolution revealed an approximately spherical three-dimensional morphology, rather than a squashed shape (Fig. S1). This morphology is expected for a membrane-bound cell inflated by osmotic pressure, and suggests that the mechanical forces from the agarose and coverslip did not substantially perturb L-form shape.

The initial periods of growth and division resulted in microcolonies of aberrantly shaped cells. To analyse these complex morphologies, we developed image-analysis algorithms that allowed us to segment each of the single cells imaged by phase-contrast microscopy and thereby analyse the outlines of large populations of cells and track them over time as they grew (Fig. 2A, Movie S3). Although we observed a diverse array of morphologies across single cells and over time, the cells nonetheless appeared more elongated over time, eventually returning to a rod-like shape.

In order to probe the mechanism underlying morphogenesis during L-form reversion, we investigated the role of the cytoskeletal protein MreB based on its importance for maintenance of rod-like growth in walled cells (Wachi *et al*., 1987). To determine whether MreB is required for reversion to a rod-like shape in L-forms, we studied the reversion process in the presence of A22, an antibiotic that inhibits MreB polymerization and localization (Gitai, 2005). Treatment of rod-shaped *E. coli* cells with A22 results in a transition to a spherical morphology over several cell cycles, and eventually leads to lysis (Furchtgott *et al*., 2011). After cefsulodin removal, we observed that L-forms growing in the presence of A22 grew to a large area and were unable to recover a rod-like morphology (Fig. 2B and C, Movie S4). Therefore, MreB is required not only for the maintenance of a rod-like shape, but also for *de novo* rod morphogenesis in *E. coli*.

To quantify the morphological features of the reversion trajectory over long periods of time, we collected large populations of cells from L-form cultures at various time points after cefsulodin removal and studied their morphologies on agarose pads. In two separate experiments, we observed quantitatively similar decreases in circularity over time (Fig. 2D), indicating the adoption of an elongated shape. After ~ 5 h, the cells reached an average circularity on par with that of a culture of rod-shaped cells grown without cefsulodin in

LFLB; this corresponds to approximately five generations, as the doubling time for rod-shaped cells in the same conditions is ~ 1 h (Fig. S2).

We next developed several local measures of cell shape in order to quantify the convergence to a rod-like shape, and found that, similar to circularity, these measures indicated convergence to a rod-like shape in approximately 5 h. Since the sides of rod-shaped cells are nearly straight, we measured the fraction of each cell contour at low curvature (radius of curvature > 8 μm), and observed an increase over time consistent with development of the lateral sides of a rod-like shape (Fig. 2E). Likewise, at the poles of a rod-shaped cell, the direction of the tangent vector of the cell contour changes rapidly over a short distance. Thus, we calculated the minimal fraction of the cell contour required for the tangent vector to reverse direction, and found that this quantity decreased over time to a value consistent with the stable development of poles of an elongated, rod-shaped cell (Fig. 2F). Finally, to quantify convergence to a uniform cell width, we employed a meshing algorithm to find the neutral axis of the cell and provide an operational measure of the width of the cell (*Experimental procedures*). Over a period of ~ 5–6 h, the variability in width, measured as the average of the standard deviation in width across the length of a single cell, converged to the value observed in a wild-type population of rod-shaped cells (Fig. 2G). By fitting the width profile of each cell to that of a rod (*Experimental procedures*), we determined that the fraction of rod-shaped cells increased over time to nearly 100% (Fig. 2H). Like circularity, all of these measures were consistent across separate experiments, measured at different time intervals. Furthermore, inhibition of MreB by A22 treatment prevented any recovery in these measures. Therefore, despite the substantial heterogeneity observed in early stages of L-form reversion, the populations followed a well-defined trajectory back to rod-like shapes, and MreB helps to guide cells along that trajectory.

Reverting L-forms maintain normal muropeptide composition

Given the diversity of morphologies during reversion (Fig. 2), we were interested in determining how quickly L-forms could recover the biochemical cell-wall composition of walled, rod-shaped cells. Previous studies indicated that stationary-phase cultures of *E. coli* L-forms harbour low levels of peptidoglycan, which exhibited reduced glycan strand length but otherwise generally resembled normal *E. coli* peptidoglycan (Joseleau-Petit *et al*., 2007). Studies of walled, approximately round mutants of *E. coli* likewise revealed little difference in muropeptide content compared to wild-type *E. coli* (Driehuis and Wouters, 1987; de Jonge, 1990). The low levels of peptidoglycan in L-forms indicates that L-forms do not contain sufficient peptidoglycan to completely enclose the cell. Thus we were further intrigued by the problem of how peptidoglycan in a reverting L-form undergoes a global topological transition as it reverts to a complete, enclosing sacculus from a fragmented initial state. Using Ultra Performance Liquid Chromatography (*Experimental procedures*), we measured the overall peptidoglycan abundance and the muropeptide composition at several time points during the reversion process (Fig. S3). Using total protein levels to normalize the muropeptide quantifications (Joseleau-Petit *et al*., 2007), we determined that overall peptidoglycan levels recover within 4 h after cefsulodin removal (Fig. 3A), somewhat faster than the morphological dynamics (Fig. 2D–H). We also quantified the dynamics of the most abundant species from several important classes of muropeptides:

monomers (uncrosslinked peptidoglycan), dimers (crosslinked peptidoglycan), trimers (highly crosslinked, possibly multilayered peptidoglycan), and anhydromuropeptides (glycan strand ends; inversely proportional to strand length). The recovery trajectories were similar for each of these muropeptide species, with dynamics similar to that of overall peptidoglycan levels (Fig. 3B). Closer inspection of minor peaks revealed that the pentapeptide monomer M5 was strongly enriched early in the reversion process (Fig. 3C), suggesting that DD-carboxypeptidase activity is inhibited in L-forms by regulation of enzymatic activity, the altered structure of the cell envelope, and/or off-target effects of cefsulodin. The reduction in M5 abundance back to the levels of rod-shaped cells during reversion coincided with an increase in the amount of tetrapeptide M4, perhaps reflecting the availability of pentapeptides for hydrolysis. There was also a coincident rise in the amount of crosslinked peptidoglycan (dimers and trimers), consistent with recovery from cefsulodin treatment. The decreasing mole fraction of the anydromuropeptide dimer D44N indicates an increasing glycan strand length over time, consistent with a previous observation of reduced strand length in *E. coli* L-forms (Joseleau-Petit *et al*., 2007). These results suggest that newly synthesized peptidoglycan in reverting L-forms resembles that of exponentially growing rod-shaped cells, and that biochemical peptidoglycan composition and abundance are not sufficient to define a rod-like morphology: cells of the same muropeptide composition can demonstrate not only radically different morphologies, but also fundamentally different peptidoglycan topology.

Residual cell wall in L-forms is localized to non-spherical regions of the cell

Previous studies have indicated that *E. coli* L-forms contain a small residual amount of cell-wall material, and that septal cell-wall synthesis is necessary for propagation (Joseleau-Petit *et al*., 2007). These results suggested that the residual cell-wall material in L-forms is located at septa. In propagating L-forms, growing with cefsulodin, cells undergoing division featured prominent septa, while cells not undergoing division were mostly round. To determine the subcellular pattern of the residual cell-wall material in propagating L-forms, we labelled L-forms with fluorescent D-amino acids (FDAAs) (Kuru *et al*., 2012; Siegrist *et al*., 2013), which are incorporated directly into the cell wall. We found that labelled material was indeed localized to the septa of dividing L-forms (Fig. 4A.i), or at morphological features that we inferred to be old division sites (Fig. 4A.ii) due to their similarity in appearance to division sites observed in time-lapse experiments. By contrast, there was no measureable FDAAsignal in L-forms with spherical morphology (Fig. 4A.iii), suggesting that L-forms do not undergo cell-wall synthesis until beginning division.

We next employed FDAA labelling to study the localization of cell-wall material in reverting L-forms. We expected that cells under turgor pressure would adopt a spherical shape unless otherwise constrained, and thus hypothesized that non-spherical, angular portions of the cell indicate the presence of cell wall. Although FDAAs are not suitable for continuous tracking of cell-wall insertion due to their rapid bleaching and low quantum yield, we were able to determine the pattern of accumulated cell-wall insertion over a period of growth. To measure the subcellular distribution of cell-wall material, we incubated reverting L-forms with FDAAs for 2 h in liquid culture. FDAAs were added immediately after cefsulodin was removed, to ensure maximal labelling of cell wall inserted during the

reversion process. When we examined the FDAA localization pattern in reverting L-forms, there was no detectable signal in spherical cells, similar to propagating L-forms. By contrast, in cells with a non-spherical region attached to a round region similar in size to propagating L-forms, we observed labelling only in the non-spherical region, consistent with our hypothesis that morphology was correlated with cell-wall growth (Fig. 4B).

We then measured the FDAA fluorescence intensity along the two-dimensional cell outlines of the cells *(Experimental procedures)* and determined the correlation of fluorescence with the curvature of the outline (Fig. 4C). Our convention is that protrusions, such as the poles of rod-shaped cells, are positively curved, while invaginations, such as the constricting region of the septa of dividing cells, are negatively curved. Spherical cells will thus have positive curvatures equal to the inverse radius of the cell. For a cell symmetric about the plane of focus, the curvature of the cell outline (a one-dimensional curve) is approximately one of the two principal curvatures of the two-dimensional cell surface, with the other corresponding to curvature along a line perpendicular to the focal plane. In a rod-shaped cell, we adopt a sign convention such that the poles of the cell have positive curvature, the septum has negative curvature, and the sides of the cell have approximately zero curvature. Since the other principal curvature is positive, the sign of the Gaussian curvature (the product of the two principal curvatures) is the same as the sign of the curvature of the cell outline. Although any sign convention for contour curvature is arbitrary, our convention has the advantage of matching the sign of the Gaussian curvature, which is non-arbitrary. Cell-wall enrichment as a function of local curvature indicated a minimum at a curvature of 1.05 μm^{-1}, corresponding to the spherical portions of the cell that remained from the initial spherical L-form (Fig. 4B and C). The mean radius of the cells (computed as $\sqrt{(A/\pi)}$, where A is the area) was 1.2 μm, yielding a curvature of 0.85 μm^{-1} (Fig. 4C, dashed line) which serves as a lower bound to the curvature of the spherical portions of the cell. Thus, our results demonstrate that deviations from spherical shape are strong indicators of the presence of cell wall, and that curvature (specifically deviations of curvature from the typical spherical L-form shape) is strongly associated with regions of cell-wall regrowth in reverting L-forms.

MreB targets cell-wall insertion to regions of negative curvature

In order to probe the coupling between MreB and cell wall synthesis, we examined how treatment with A22 alters the subcellular distribution of cell wall in reverting L-forms. Although disruption of MreB with A22 prevents the establishment of a rod-like shape, L-forms still appeared to regrow a cell wall, based on their apparent rigidity when growing in close contact on a surface (Fig. 2B). Using FDAA labelling, we verified that cell-wall material was present after 4 h of growth (Fig. 4D). Therefore, L-forms can regrow a cell wall in the presence ofA22, although they do not revert to a rod-like morphology.

Since L-forms regrow cell wall in the absence of intact MreB polymers, but cannot generate a rod-like morphology, we hypothesized that MreB drives morphogenesis by spatially regulating cell-wall synthesis. To test this hypothesis, we examined the distribution of FDAA fluorescence in reverting L-forms in the presence ofA22. In these L-forms, there was depletion of cell-wall label at regions of negative curvature (Fig. 4C), in contrast to

untreated L-forms. Therefore, we infer that intact MreB polymers target new cell-wall material to regions of negative curvature. Furthermore, in the absence of MreB, cell wall synthesis continues to occur, but appears to be uncoordinated.

MreB localizes to negatively curved regions of reverting L-forms

Since MreB causes enrichment of cell-wall material at sites of negative curvature, we hypothesized that MreB would also be enriched at these sites. To examine MreB localization, we utilized an *E. coli* MG1655 strain containing a single copy of *mreB* fused internally to the fluorescent protein mVenus at residues G228 and D229, integrated into the chromosome at the native *mreB* locus (Ursell *et al*., 2014). Cells expressing this sandwich fusion grew at the same rate and closely approximated the cell morphology of the unlabelled strain; walled $MreB^{sw}$-mVenus cells are slightly wider than unlabelled cells (Ursell *et al*., 2014). We measured the distribution of MreB fluorescence along the cell outline using the same method used to quantify cellwall enrichment (*Experimental procedures*). To quantitatively determine whether MreB displayed a localization preference, we computed enrichment in fluorescent intensity as a function of curvature. This calculation revealed that MreB localization was enriched at regions of negative curvature, and depleted at regions of positive curvature. This pattern was apparent in both single cells (Fig. 5A and B) and when the data were averaged over time-lapse movies of the growth of different cells ($n = 3$, Fig. 5C). Since our measurements focused on the fluorescence signal and the two-dimensional curvature along the cell outline in the image focal plane, we also labelled the cells with the membrane dye FM4–64 to ascertain whether the unobserved, three-dimensional aspects of the cell geometry or our method of fluorescence integration (*Experimental procedures*) were likely to affect the MreB enrichment profile. In contrast to the MreB fluorescence signal, the FM4–64 signal displayed a localization pattern that was essentially curvature independent, indicating that the enrichment we observed was not due to geometric effects or to imaging artefacts.

Because the morphology of the L-forms changed dramatically over the course of reversion to a rod-like shape, we were interested in whether the MreB enrichment profile changed over time. We sorted each of our single-cell enrichment profiles for time-lapse movies of 13 cells into time intervals measured relative to the removal of cefsulodin. We found that the enrichment of MreB to regions of negative curvature was rapidly established as the cell began to develop a non-uniform shape, and persisted through several divisions (Fig. 5D). For the first 25 min of reversion, there was little heterogeneity in curvature against which to measure differential localization (Fig. 5E). After heterogeneities in curvature were established at ~ 25 min, the enrichment pattern remained essentially static, except for greater sampling of negative curvature values. Given that morphology changed substantially over the time-course of these observations, this rapid establishment of a specific pattern of curvature-based enrichment is consistent with MreB localization driven by equilibrium membrane binding of MreB with a curvature-dependent binding energy, in which the localization pattern is established via the rapid timescales of membrane binding/unbinding and diffusion.

To further explore the relationship between MreB localization and cell shape, we computed the cross-correlation between MreB and contour curvature in order to see if one signal arrived before the other. This cross-correlation analysis confirmed the association between MreB and negative curvature, and did not exhibit an observable time lag, indicating that the appearance of MreB was coincident with changes in curvature, within the spatiotemporal resolution of our measurements (Fig. S4). Because diffraction limits our ability to measure short-wavelength fluctuations in the cell outline, we cannot rule out the possibility of a time lag between the arrival of MreB and such fine-scale curvature. This result is consistent with a model of feedback between MreB localization and cell curvature in which MreB localizes to regions of negative curvature and directs local cell-wall insertion that modulates cell curvature.

To explore a causal relationship between MreB localization and contour curvature, we probed temporal dynamics by examining the autocorrelation functions of those two signals (Fig. 5F). In particular, the timescales associated with the decay of the autocorrelation measure the persistence of information contained in each signal. The curvature autocorrelation function was well fit by a single exponential, indicating a single dominant timescale in cell-shape dynamics of 24.5 min (95% confidence interval: [23.7, 25.2]) for reduction of the autocorrelation function by a factor of *e*, in reasonable agreement with the timescale over which cells grew and change shape (Fig. 2). This timescale reflects changes in shape on length scales above the diffraction limit. In contrast, the MreB autocorrelation function was poorly fit by a single exponential, but was well fit by the sum of two exponentials, revealing a fast timescale of 2.1 min (95% confidence interval: [1.9, 2.3]) and a slow timescale of 28.7 min (95% confidence interval: [27.2, 30.2]). We interpret the fast timescale as the persistence time of an MreB cluster near a given membrane location; the slow timescale is similar to the curvature autocorrelation timescale, as one would expect given the observed cross-correlation between MreB fluorescence and curvature. Thus, MreB localization varies much more rapidly than cell shape. One explanation for the observed curvature-MreB correlation is that MreB recruits cell-wall synthesis, which in turn induces negative curvature. However, in this model, one would expect MreB to persist at least as long as changes in cell shape, while our experimental evidence demonstrates that MreB varies on a timescale an order of magnitude faster. Taken together, the MreB fluorescence patterns indicate dynamic targeting of growth to regions of negative curvature, which is critical for the regeneration of rod-like shapes.

FtsZ localizes predominantly to constricting septa in reverting L-forms but not to all sites of negative curvature

Another factor that has been proposed to dictate large-scale shape changes during *de novo* rod-like morphogenesis is septal invagination at division sites (Ranjit and Young, 2013). These division-related invaginations are mediated by the cytoskeletal protein FtsZ (Hsin *et al*., 2012; Li *et al*., 2013) and by FtsI-mediated cell-wall synthesis (Botta and Park, 1981; Hedge and Spratt, 1985). We therefore utilized the plasmid pCA24N-ftsZ (Kitagawa *et al*., 2005) expressing a C-terminal fusion of FtsZ to green fluorescent protein (GFP) to visualize the localization of FtsZ during L-form reversion. As expected, FtsZ–GFP was localized at division sites, and the FtsZ-ring gradually contracted along with increases in constriction

(Fig. 6A). In contrast, FtsZ appeared absent from regions of the cells away from these division sites, which were nevertheless concurrently reshaped to exhibit regions of negative curvature (Fig. 6B). Thus, although FtsZ and the division machinery appear to contribute to some – but not all – large-scale changes in the shape of the cell and septal cell wall, the divisome alone is insufficient for *de novo* rod morphogenesis. An additional mechanism, such as the curvature-mediated patterning of cell-wall synthesis by MreB, is required for some of the large-scale changes in shape required for *de novo* rod morphogenesis.

Discussion

How is cell shape programmed in bacteria? This question is intimately tied to the spatiotemporal regulation of cellwall synthesis. Our experiments demonstrate that a spherical, cell-wall-deficient *E. coli* (the L-forms described here) can rapidly regrow its wall and regenerate its bacillary shape in an MreB-dependent manner. In particular, the conserved morphological features of the trajectories of populations of reverting L-forms suggest that the cellwall synthesis machinery can measure cell geometry in order to direct new synthesis to the appropriate locations. Quantification of the subcellular localization of cell-wall insertion and of MreB indicated that the process of reversion to a rod-like shape requires localization of MreB to negatively curved regions of the cell (Fig. 5C), which in turn drives synthesis of new cell wall (Fig. 4C) with spatiotemporal dynamics consistent with the production of rods over the course of a few divisions (Fig. 2).

Our findings suggest that MreB may be measuring the shape of the cell by sensing the curvature (and thus the local radius), and thereby coordinating cell-wall synthesis. We have previously observed similar curvature-dependent localization of MreB during regular growth of rod-shaped growth, and we have used computational simulations to demonstrate that a curvature-dependent bias in insertion of new peptidoglycan promotes maintenance of a rod-like shape in walled cells (Ursell *et al*., 2014). However, from this previous work in rod-shaped cells, it is unclear whether curvature-dependent localization is responsible for maintenance of a rod-like shape, as a sort of geometric proofreading, or if this localization is how a rod-like shape is established in the first place. This work suggests the latter: curvature-dependent localization of MreB is involved in the early stages of rod morphogenesis.

The association between the presence of MreB and the negative curvature of the cell is consistent with several models for the interaction between cell shape and cell-wall synthesis. MreB could localize in response to an unknown variable and then direct a pattern of cell-wall synthesis that, in turn, generates negative curvature due to the presence of rigid cell-wall material. Although the constriction sites where FtsZ is localized also have negative curvature (Fig. 6), cells exhibit other regions of negative curvature that appear to lack FtsZ. Alternatively, MreB could localize in response to cell curvature, perhaps by biophysical mechanisms such as a curvature-dependent binding energy, as investigated in other important biological systems (Peter *et al*., 2004; Ramamurthi and Losick, 2009). Finally, both MreB and curvature could be driven by the same signal, for instance the presence of other proteins involved in cell wall synthesis. We have presented evidence arguing against the first model alone: MreB is much more dynamic than the changes in cell shape (Fig. 5F).

Furthermore, analysis of the cross-correlation of curvature and MreB signals revealed no measurable lag or lead between the two signals (Fig. S4); if MreB localization preceded measurable changes in shape, this lag should have been detectable, since MreB localization is fast while cell-shape changes occur slowly. Our observation of no lag or lead is consistent with a model in which MreB localizes rapidly in response to curvature but also drives subsequent changes in curvature via cell-wall insertion. Regardless, the patterning of cell-wall insertion by MreB is critical for the evolution of the curvature distribution towards a rod-like shape.

Previous studies of *E. coli* cells after morphological or cell-wall perturbation have elucidated several strategies that might be important for the recovery of a rod-like shape. Lysozyme-induced spheroplasts adopt a spherical morphology similar to our L-forms that likewise revert to a rod-like shape upon removal of lysozyme (Ranjit and Young, 2013). Morphological reversion in these cells appears to rely on division, during which defects such as branches introduced in early divisions eventually become propagating, rod-shaped cells. Although our data indicate that septal cell-wall synthesis is critical for the propagation of L-forms (Fig. 4A), substantial geometric changes occurred prior to the first cell division after cefsulodin removal (Fig. 2A), indicating that partial morphological reversion can occur without division in our experiments. These distinctions could be due to underlying differences in the initial states prior to reversion, such as differences in the amount of peptidoglycan or different wash-out kinetics of lysozyme compared with those of covalently bound cefsulodin. For the Gram-negative, crescent-shaped bacterium *C. crescentus*, A22 treatment disrupts MreB function and results in a lemon shape; after removal of A22, these cells undergo extensive changes including cell thinning, branching, and possibly thickening of their cell wall during the transition back to a rod-like morphology (Wagner *et al*., 2005; Takacs *et al*., 2010). A common theme that emerges from these studies is that bacteria use elements of the same machinery that maintains rod-like growth to initiate rod-like shapes. Future investigations may help to clarify whether the elements of rod-shape establishment that have been uncovered are general or specific to particular initial states.

In addition to MreB, several other proteins have been implicated in rod-shape determination in *E. coli*, such as RodZ (Bendezu *et al*., 2009), PBP2 (Spratt, 1977), and RodA (Iwaya *et al*., 1978). Dissecting the complex set of interactions among these proteins, MreB, and the rest of the cell-wall synthesis machinery may be facilitated by studies of L-form propagation and reversion in targeted mutants, and may determine whether other morphogenetic proteins are responsible for the localization of MreB. Peptidoglycan composition is similar throughout the reversion process, and levels of peptidoglycan similar to those of walled cells are established prior to re-establishment of a rod-like shape (Fig. 3A), indicating that the spatial organization of the synthesis machinery, rather than its biochemical output, is more important for shape determination in L-forms. Studies of reversion in other rod-shaped organisms such as the eukaryote *Schizosaccharomyces pombe* (Kelly and Nurse, 2011) will help to elucidate general principles of *de novo* wall synthesis and morphogenesis.

It will be interesting to compare our data with measurements from non-rod-shaped species to determine whether rods are easier to regenerate than other shapes. To date, however, it has been challenging to directly observe reversion of L-forms from Gram-positive bacteria due

to the low frequency of reversion; without direct visualization, any potential reversion events require extreme care to ensure that no walled cells were present at the start of the experiment. Nevertheless, there is strong indirect evidence that L-forms of *B. subtilis* are capable of reverting to a rod-like morphology (Kawai *et al*., 2014). High-throughput imaging of a large field of view may facilitate the direct observation of these rare events. The thicker wall of Gram-positive bacteria may make L-form reversion more difficult due to the need for more extensive wall synthesis; if this is the case, the trajectory of wall regrowth may help to shed light on the regulation of cell-wall thickness in these organisms. Furthermore, L-form reversion may elucidate how specific shapes developed over evolutionary timescales. For the *E. coli* L-form reversion we have investigated here, rods can be rapidly generated from a sphere within a few generations, and without requiring significant changes in cell size during reversion (Fig. 2C). These observations suggest that small genetic perturbations could in principle result in drastic alterations in morphology. The dramatic ability of bacteria to engineer precise shapes from a blank slate suggests that this global and complex cellular feature is nevertheless guided by fundamental physical principles.

Experimental procedures

Strains

Escherichia coli MG1655 and *E. coli* MG1655 $MreB^{sw}$-mVenus were grown without selective antibiotics. *E. coli* MG1655 pCA24N-ftsZ was grown in 10 μg ml^{-1} chloramphenicol to prevent plasmid loss; leaky expression from the T5-*lac* promoter in the absence of isopropyl β-D-1-thiogalactopyranoside provided adequate expression of FtsZ–GFP without inducing lethality due to overexpression (Kitagawa *et al*., 2005).

Growth of L-forms

Overnight cultures of the appropriate strain were diluted 1:100 into 5 ml LFLB, which is lysogeny broth (LB), Lennox formulation (5 g l^{-1} NaCl), supplemented with 3.6% sucrose and 10 mM $MgSO_4$. The cultures were then incubated at 37°C for 1 h, at which point cefsulodin was added to a final concentration of 60 μg ml^{-1}; cells were then incubated overnight with shaking at 30°C. For reversion experiments, L-forms were washed twice in LFLB with centrifugation at 10 000 *g* for 4 min, followed by resuspension in LFLB. For experiments in liquid culture, washed L-forms were diluted into LFLB (for growth up to 5 h, a 1:10 dilution was used; for growth times greater than 5 h, a 1:100 dilution was used). Where indicated, A22 was added to agarose to a final concentration of 10 μg ml^{-1} immediately before casting the pad. In liquid cultures, an A22 concentration of 30 μg ml^{-1} was used.

Imaging

Cells were imaged on an inverted fluorescence microscope with a 100× (NA 1.40) oil-immersion objective. Images were collected on an electron multiplying charged couple device camera using μManager version 1.3 (http://www.micro-manager.org) (Edelstein *et al*., 2010). Cells were maintained at 30°C during imaging with an active-control environmental chamber (HaisonTech, Taipei, Taiwan).

For experiments on agarose pads, 2 μl of washed L-forms were spotted onto a pad of 1% agarose in LFLB. Pads were formed in FastWells (Grace Bio-Labs, Bend, OR, USA) to allow for gas exchange during imaging. In Fig. 1, the experiments were performed in Onix B04A microfluidic chips (CellAsic, Hayward, CA, USA). Exponentially growing, rod-shaped cells were loaded into the imaging chamber, and media reservoirs were filled with LFLB and LFLB + cefsulodin.

Growth rates

Overnight cultures were back-diluted 1:1000 into 200 μl LFLB and grown with shaking at 30°C in a plate reader. At 7.5 min intervals, the absorbance at wavelength 600 nm was measured. The natural logarithm of the optical density was fit to the Gompertz equation (Zwietering *et al*., 1990) in order to determine a maximum specific growth rate, and from that, the doubling time. Each growth curve was fit individually, and the fitting parameters were averaged in order to generate an average fit.

Image analysis

Time-lapse and static images were segmented using a custom MATLAB software package (Ursell *et al*., 2014). To ensure the accuracy of segmentation of static images, cell outlines from all time points and experimental conditions in a given experiment were pooled and examined in random order for contour accuracy and phase density, without user knowledge of the time point or experimental condition. To determine cell lineages, a reverse-tracking approach was used: starting from the final frame analysed, each cell's predecessor was found by searching for the cell in the previous frame that had the greatest area overlap with the cell in the current frame.

The turning radius of the cell was measured by finding the shortest contour distance over which the cosine of the angle between contour tangent vectors was less than −0.9 (154 degrees). Width measurements were made using the MicrobeTracker meshing algorithm (Sliusarenko *et al*., 2011). Meshes were accepted if the regions defined by the mesh accounted for at least 95% of cell area and had a maximum spacing of 5 pixels (0.4 μm). To fit width profiles to a rod-like morphology, the polar regions of 285 rod-shaped cells were measured and pooled to determine the average shape of an *E. coli* pole. For fitting each cell, the maximum width was measured along with the length and a new comparison profile was constructed with the same maximum width and length, using the measured average pole shape at the ends of the profile and a constant width between the poles. In Fig. 2H, a cell was considered rod-shaped if the mean squared deviation from the comparison profile was less than 0.05 μm^2, the aspect ratio was greater than 2.0, and the meshing algorithm succeeded; 98% of all rod-shaped cells met these criteria.

Measurement of fluorescence profiles

To measure fluorescence profiles along cell outlines, we segmented time-lapse videos as described above, and constructed vectors normal to each cell outline at points along the contour with a spacing of 1 pixel (0.08 μm). We then integrated the fluorescence intensity along these normal directions for a distance of 3 pixels (0.24 μm) inside the cell. This method avoided the introduction of geometric biases, unlike straightforward area

integration, which employs a smaller area element for regions of positive curvature. Enrichment profiles were computed for each cell and time point by dividing the measured fluorescent signal at each contour point by the mean of that signal over all contour points of the same cell and time point. For FDAA labelling, mean intensities were small, and therefore a small constant was added to prevent division by a number close to zero. Where indicated, multiple cells were pooled by combining all contour points and their corresponding enrichment, and statistics such as means and standard errors were computed on a per-contour-point basis.

Construction of kymographs and temporal correlation analysis

To generate kymographs, we used a cross-correlation-based approach to align curvature profiles from one frame to the next, and used the alignment computed from the curvature profile to align the fluorescence profile. Auto- and cross-correlations were computed from the aligned kymographs: first, curvature and fluorescence profiles were re-sampled to allow for comparison between different time points in which cell perimeter varied. The cross-correlation at each contour point was then averaged across cells.

Peptidoglycan analysis

At 45-min intervals, samples from an overnight culture of L-forms were washed twice with centrifugation at 10 000 *g*, diluted 1:10 into 250 ml LFLB, and incubated with shaking at 30°C. 260 min after the start of washing the first culture, all samples, along with 250 ml of L-forms from an overnight culture, were centrifuged, resuspended, and lysed in boiling 6% sodium dodecyl sulphate. An additional sample of *E. coli* MG1655, growing exponentially LB at 37°C at an OD_{600} of ~ 0.5, was also prepared as a positive control and as a point of comparison for peptidoglycan content; previous studies have noted that temperature has little effect on muropeptide composition (Glauner *et al*., 1988; de Jonge, 1990). After boiling, the protein content of each sample, as well as the baseline protein content of the LFLB and LB media, was measured using the Bio-Rad DC Protein Assay (Bio-Rad, Hercules, CA, USA). After measuring protein levels, the peptidoglycan was purified, digested, and quantified via Ultra Performance Liquid Chromatography as reported previously (Desmarais *et al*., 2014). Chromatogram baselines were obtained by computing the second percentile of the chromatogram in sliding 1.66 min windows, followed by smoothing with the Whittaker algorithm (Eilers, 2003). The estimated baseline was subtracted from the chromatogram, and the process was iterated 200 times (Fig. S3). Relative peptidoglycan levels were computed by integrating the baseline-subtracted chromatograms for each sample and dividing by the baseline-subtracted protein levels. Individual peaks were integrated by least-squares fitting of each peak to a Gaussian profile.

Labelling of cell wall and membrane

FDAA labelling was performed in 100 μl cultures containing 1% dimethyl sulphoxide and 0.5 mM of the fluorescent D-amino acid HADA, along with cefsulodin or A22 as appropriate. L-forms were grown in this medium with shaking at 30°C, then washed four times with centrifugation at 10 000 *g* for 4 min, followed by resuspension in LFLB. Cell membranes were labelled by including 2 μg ml^{-1} FM4–64 in the agarose pads.

Supplementary Material

Refer to Web version on PubMed Central for supplementary material.

Acknowledgments

This work was supported by a National Science Foundation Graduate Research Fellowship (to G.B.), National Science Foundation Award PHY-0844466 (to J.S.), National Science Foundation CAREER Award MCB-1149328 (to K.C.H.), and National Institute of Health Director's New Innovator Award DP2OD006466 (to K.C.H.). This work was also supported in part by the National Science Foundation under Grant PHYS-1066293 and the hospitality of the Aspen Center for Physics. The authors thank members of the Huang lab for insightful discussions, Felipe Bendezú and Piet de Boer for assistance with strain construction, Russell Monds and Selwyn Quan for providing the MreB-mVenus fusion, and Erkin Kuru, Yves Brun, and Michael VanNieuwenhze for their generous gift of fluorescent D-amino acids.

References

Bendezu FO, Hale CA, Bernhardt TG, de Boer PA. RodZ (YfgA) is required for proper assembly of the MreB actin cytoskeleton and cell shape in *E. coli*. EMBO J. 2009; 28:193–204. [PubMed: 19078962]

Botta GA, Park JT. Evidence for involvement of penicillin-binding protein-3 in murein synthesis during septation but not during cell elongation. J Bacteriol. 1981; 145:333–340. [PubMed: 6450748]

Desmarais SM, Cava F, de Pedro MA, Huang KC. Isolation and preparation of bacterial cell walls for compositional analysis by ultra performance liquid chromatography. J Vis Exp. 2014; (83):e51183.10.3791/51183 [PubMed: 24457605]

Dominguez-Cuevas P, Mercier R, Leaver M, Kawai Y, Errington J. The rod to L-form transition of *Bacillus subtilis* is limited by a requirement for the protoplast to escape from the cell wall sacculus. Mol Microbiol. 2012; 83:52–66. [PubMed: 22122227]

Dominguez-Escobar J, Chastanet A, Crevenna AH, Fromion V, Wedlich-Soldner R, Carballido-Lopez R. Processive movement of MreB-associated cell wall biosynthetic complexes in bacteria. Science. 2011; 333:225–228. [PubMed: 21636744]

Driehuis F, Wouters JT. Effect of growth rate and cell shape on the peptidoglycan composition in *Escherichia coli*. J Bacteriol. 1987; 169:97–101. [PubMed: 3539928]

Edelstein, A.; Amodaj, N.; Hoover, K.; Vale, R.; Stuurman, N. Computer Control of Microscopes Using μManager. New York: John Wiley & Sons; 2010.

Eilers PH. A perfect smoother. Anal Chem. 2003; 75:3631–3636. [PubMed: 14570219]

Furchtgott L, Wingreen NS, Huang KC. Mechanisms for maintaining cell shape in rod-shaped Gram-negative bacteria. Mol Microbiol. 2011; 81:340–353. [PubMed: 21501250]

Garner EC, Bernard R, Wang W, Zhuang X, Rudner DZ, Mitchison T. Coupled, circumferential motions of the cell wall synthesis machinery and MreB filaments in *B. subtilis*. Science. 2011; 333:222–225. [PubMed: 21636745]

Gitai Z. The new bacterial cell biology: moving parts and subcellular architecture. Cell. 2005; 120:577–586. [PubMed: 15766522]

Gitai Z, Dye N, Shapiro L. An actin-like gene can determine cell polarity in bacteria. Proc Natl Acad Sci USA. 2004; 101:8643–8648. [PubMed: 15159537]

Glauner B, Holtje JV, Schwarz U. The composition of the murein of *Escherichia coli*. J Biol Chem. 1988; 263:10088–10095. [PubMed: 3292521]

Goodell EW, Lopez R, Tomasz A. Suppression of lytic effect of beta lactams on *Escherichia coli* and other bacteria. Proc Natl Acad Sci USA. 1976; 73:3293–3297. [PubMed: 9642]

Hedge PJ, Spratt BG. Resistance to beta-lactam antibiotics by re-modelling the active-site of an *Escherichia-coli* penicillin-binding protein. Nature. 1985; 318:478–480. [PubMed: 3906408]

Holtje JV. Growth of the stress-bearing and shape-maintaining murein sacculus of *Escherichia coli*. Microbiol Mol Biol Rev. 1998; 62:181–203. [PubMed: 9529891]

Hsin J, Gopinathan A, Huang KC. Nucleotide-dependent conformations of FtsZ dimers and force generation observed through molecular dynamics simulations. Proc Natl Acad Sci USA. 2012; 109:9432–9437. [PubMed: 22647609]

Huang KC, Mukhopadhyay R, Wen BN, Gitai Z, Wingreen NS. Cell shape and cell-wall organization in Gram-negative bacteria. Proc Natl Acad Sci USA. 2008; 105:19282–19287. [PubMed: 19050072]

Huang KC, Ehrhardt DW, Shaevitz JW. The molecular origins of chiral growth in walled cells. Curr Opin Microbiol. 2012; 15:707–714. [PubMed: 23194654]

Iwaya M, Goldman R, Tipper DJ, Feingold B, Strominger JL. Morphology of an *Escherichia-coli* mutant with a temperature-dependent round cell-shape. J Bacteriol. 1978; 136:1143–1158. [PubMed: 363690]

de Jonge BL. Isogenic variants of *Escherichia coli* with altered morphology have peptidoglycan with identical muropeptide composition. J Bacteriol. 1990; 172:4682–4684. [PubMed: 2198272]

Joseleau-Petit D, Liebart JC, Ayala JA, D'Ari R. Unstable *Escherichia coli* L forms revisited: growth requires peptidoglycan synthesis. J Bacteriol. 2007; 189:6512–6520. [PubMed: 17586646]

Kawai Y, Mercier R, Errington J. Bacterial cell morphogenesis does not require a preexisting template structure. Curr Biol. 2014; 24:863–867. [PubMed: 24704074]

Kelly FD, Nurse P. *De novo* growth zone formation from fission yeast spheroplasts. PLoS ONE. 2011; 6:e27977. [PubMed: 22194800]

Kitagawa M, Ara T, Arifuzzaman M, Ioka-Nakamichi T, Inamoto E, Toyonaga H, Mori H. Complete set of ORF clones of *Escherichia coli* ASKA library (a complete set of *E. coli* K-12 ORF archive): unique resources for biological research. DNA Res. 2005; 12:291–299. [PubMed: 16769691]

Klieneberger E. The natural occurrence of pleuropneumonia-like organisms in apparent symbiosis with *Streptobacillus moniliformis* and other bacteria. J Pathol Bacteriol. 1935; 40:93–105.

Kuru E, Hughes HV, Brown PJ, Hall E, Tekkam S, Cava F, et al. *In situ* probing of newly synthesized peptidoglycan in live bacteria with fluorescent D-amino acids. Angew Chem Int Ed Engl. 2012; 51:12519–12523. [PubMed: 23055266]

Leaver M, Dominguez-Cuevas P, Coxhead JM, Daniel RA, Errington J. Life without a wall or division machine in *Bacillus subtilis*. Nature. 2009; 457:849–853. [PubMed: 19212404]

Lederberg J. Bacterial protoplasts induced by penicillin. Proc Natl Acad Sci USA. 1956; 42:574–577. [PubMed: 16589908]

Li Y, Hsin J, Zhao L, Cheng Y, Shang W, Huang KC, et al. FtsZ protofilaments use a hinge-opening mechanism for constrictive force generation. Science. 2013; 341:392–395. [PubMed: 23888039]

Noguchi H, Matsuhashi M, Mitsuhashi S. Comparative studies of penicillin-binding proteins in *Pseudomonas aeruginosa* and *Escherichia coli*. Eur J Biochem. 1979; 100:41–49. [PubMed: 114388]

Onoda T, Oshima A, Nakano S, Matsuno A. Morphology, growth and reversion in a stable L-form of *Escherichia-coli*-K12. J Gen Microbiol. 1987; 133:527–534. [PubMed: 3309159]

Onwuamaegbu ME, Belcher RA, Soare C. Cell wall-deficient bacteria as a cause of infections: a review of the clinical significance. J Int Med Res. 2005; 33:1–20. [PubMed: 15651712]

Peter BJ, Kent HM, Mills IG, Vallis Y, Butler PJ, Evans PR, McMahon HT. BAR domains as sensors of membrane curvature: the amphiphysin BAR structure. Science. 2004; 303:495–499. [PubMed: 14645856]

Pierce CH. *Streptobacillus moniliformis*, its associated L1 form, and other pleuropneumonia-like organisms. J Bacteriol. 1942; 43:780.

Ramamurthi KS, Losick R. Negative membrane curvature as a cue for subcellular localization of a bacterial protein. Proc Natl Acad Sci USA. 2009; 106:13541–13545. [PubMed: 19666580]

Ranjit DK, Young KD. The Rcs stress response and accessory envelope proteins are required for *de novo* generation of cell shape in *Escherichia coli*. J Bacteriol. 2013; 195:2452–2462. [PubMed: 23543719]

Scheffers DJ, Pinho MG. Bacterial cell wall synthesis: new insights from localization studies. Microbiol Mol Biol Rev. 2005; 69:585–607. [PubMed: 16339737]

Shih YL, Kawagishi I, Rothfield L. The MreB and Min cytoskeletal-like systems play independent roles in prokaryotic polar differentiation. Mol Microbiol. 2005; 58:917–928. [PubMed: 16262780]

Siegrist MS, Whiteside S, Jewett JC, Aditham A, Cava F, Bertozzi CR. D-amino acid chemical reporters reveal peptidoglycan dynamics of an intracellular pathogen. ACS Chem Biol. 2013; 8:500–505. [PubMed: 23240806]

Sliusarenko O, Heinritz J, Emonet T, Jacobs-Wagner C. High-throughput, subpixel precision analysis of bacterial morphogenesis and intracellular spatio-temporal dynamics. Mol Microbiol. 2011; 80:612–627. [PubMed: 21414037]

Spratt BG. Mechanism of action of mecillinam. J Antimicrob Chemother. 1977; 3:13–19. [PubMed: 330482]

Takacs CN, Poggio S, Charbon G, Pucheault M, Vollmer W, Jacobs-Wagner C. MreB drives *de novo* rod morphogenesis in *Caulobacter crescentus* via remodeling of the cell wall. J Bacteriol. 2010; 192:1671–1684. [PubMed: 20023035]

van Teeffelen S, Wang S, Furchtgott L, Huang KC, Wingreen NS, Shaevitz JW, Gitai Z. The bacterial actin MreB rotates, and rotation depends on cellwall assembly. Proc Natl Acad Sci USA. 2011; 108:15822–15827. [PubMed: 21903929]

Ursell TS, Nguyen J, Monds RD, Colavin A, Billings G, Ouzounov N, et al. Rod-like bacterial shape is maintained by feedback between cell curvature and cytoskeletal localization. Proc Natl Acad Sci USA. 2014; 111:E1025–E1034. [PubMed: 24550515]

Wachi M, Doi M, Tamaki S, Park W, Nakajima-Iijima S, Matsuhashi M. Mutant isolation and molecular cloning of *mre* genes, which determine cell shape, sensitivity to mecillinam, and amount of penicillin-binding proteins in *Escherichia coli*. J Bacteriol. 1987; 169:4935–4940. [PubMed: 2822655]

Wagner JK, Galvani CD, Brun YV. *Caulobacter crescentus* requires RodA and MreB for stalk synthesis and prevention of ectopic pole formation. J Bacteriol. 2005; 187:544–553. [PubMed: 15629926]

Young KD. The selective value of bacterial shape. Microbiol Mol Biol Rev. 2006; 70:660–703. [PubMed: 16959965]

Zwietering MH, Jongenburger I, Rombouts FM, van't Riet K. Modeling of the bacterial growth curve. Appl Environ Microbiol. 1990; 56:1875–1881. [PubMed: 16348228]

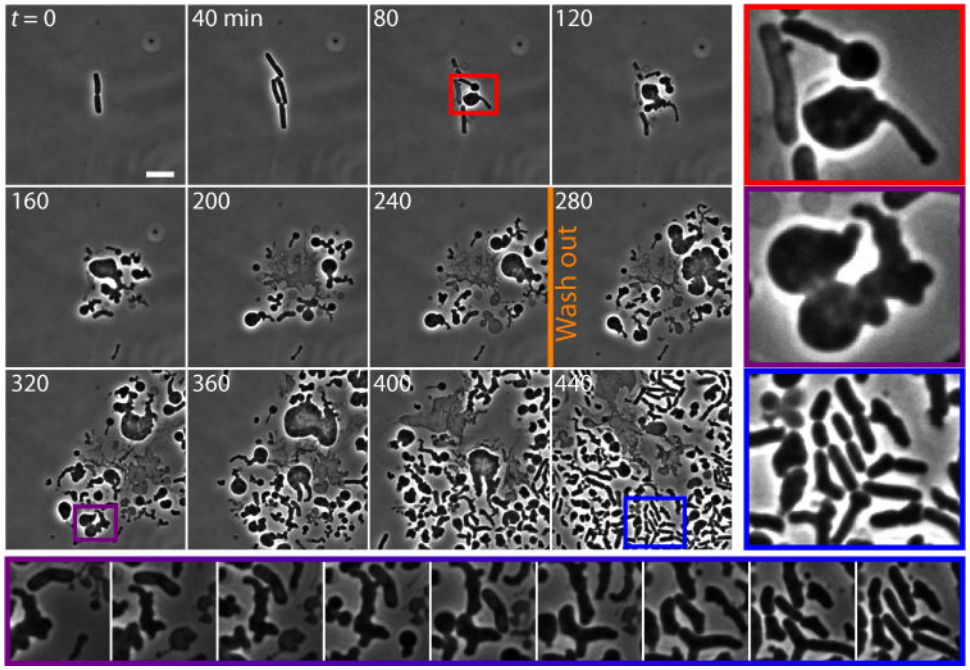

Fig. 1.

Cefsulodin treatment generates stable L-forms, which revert back to a rod-like shape when the antibiotic is removed. Phase-contrast images of cell growth in a microfluidic chamber. *E. coli* cells treated with cefsulodin develop into round L-forms (red inset), many of which are capable of propagation and proliferation. Upon removal of the cefsulodin (240 min, orange line), the viable L-forms undergo a combination of cylindrical protrusions (purple inset, right) and cytokinesis as they revert to a rod-like morphology (blue inset, right). Bottom inset: enlarged view of the development of rod-shaped cells from t = 320 min to t = 440 min. See also Movie S1. Scale bar: 5 μm.

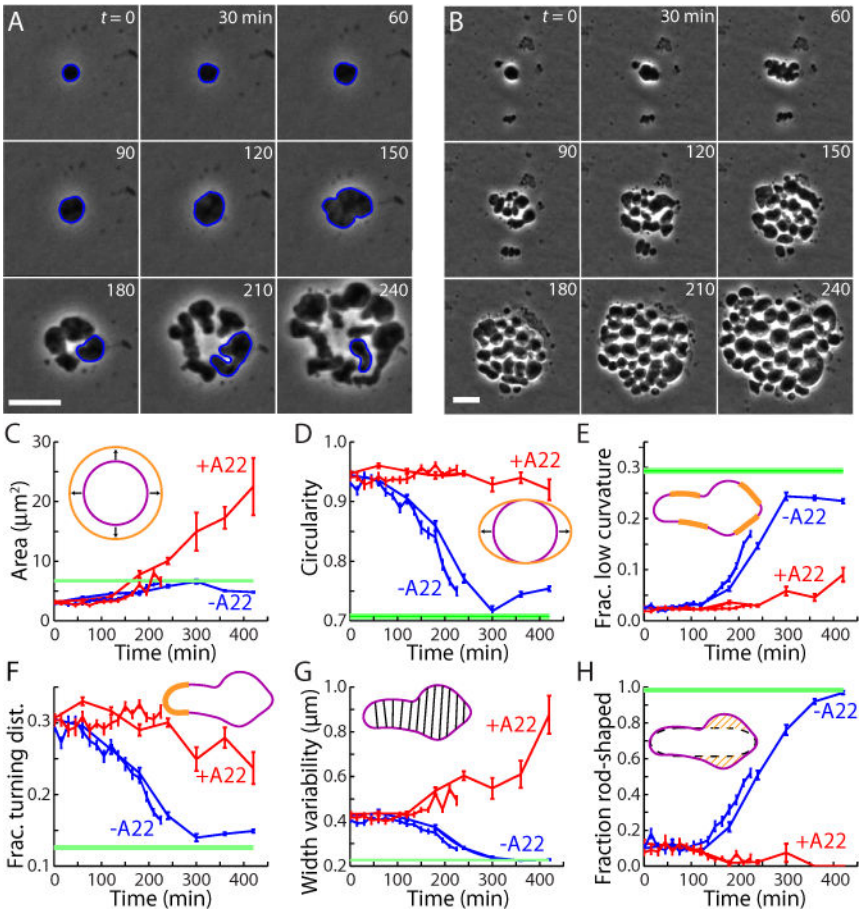

Fig. 2.

Cell-shape dynamics indicate that MreB is critical for establishment of rod-like shape during L-form reversion.

A. A cell lineage segmented from an L-form colony during reversion without A22 (blue outlines). See also Movies S2 and S3. Scale bar: 5 μm.

B. Cells within an L-form colony reverting in the presence of 10 μg ml^{-1} of the MreB inhibitor A22 develop into large, spherical cells, in contrast to the colony in (A). Scale bar: 5 μm.

C–H. Morphological measures demonstrating the convergence of reverting L-forms to a rod-like morphology, and the failure to converge during A22 treatment. Blue/red curves: L-forms reverting without/with A22 respectively. Green: measurement of exponentially growing rod-shaped cells in LFLB. Each curve is a biological replicate, measured at different time intervals, and each data point indicates the mean across all cells in the population segmented at each time point. The number of cells measured per time point ranged from n = 18–706 cells, with a mean of 250. Error bars are standard error of the mean. Error bars for measurements of rod-shaped cells are indicated by light green lines; due to the regularity of rod-shaped cells, most of these lines overlap. The doubling time in these growth conditions is 1 h.

C. The area of reverting L-forms increases slightly in the absence of A22, and approaches the area of wild-type cells in LFLB over the course of ~ 4–5 h. In contrast, A22 treatment leads to cells with areas that continue to increase over time.

D. The circularity ($\sqrt{4\pi A}/p$, where A and p are cell area and perimeter, respectively, with a maximum value of one for a circular cell) of reverting cells decreases over time as cells become more rod-like, while the contour of A22-treated cells remains roughly circular.

E. The fraction of contour segments at small curvature increases in reverting L-forms, indicating the development of straight-sided cells. L-forms do not develop straight sides in the presence of A22.

F. Normalized turning radius of cell contours decreases in reverting L-forms, indicating development of pole-like regions. A22-treated cells do not develop poles, as the turning radius remains a constant fraction of the contour length.

G. Intracell standard deviation in width decreases in reverting L-forms, while A22-treated L-forms exhibit increased width variability over time.

H. The fraction of rod-shaped cells in a culture of reverting L-forms increases over time; A22 prevents the appearance of rod-shaped cells.

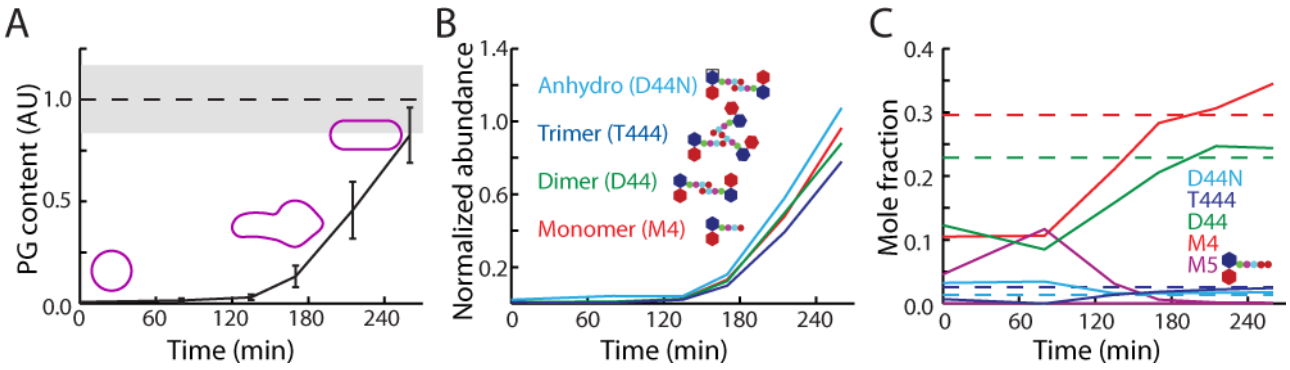

Fig. 3.

Muropeptide analysis of reverting L-forms via Ultra Performance Liquid Chromatography reveals normal peptidoglycan composition during reversion.

A. Changes in cellular peptidoglycan (PG) content over time (total integrated muropeptide Ultra Performance Liquid Chromatography signal normalized by protein concentration) reveals recovery of the cell wall to normal levels within 4 h. Dashed line and grey region show PG content of exponentially growing, rod-shaped cells along with estimated error. Error bars were computed from standard deviation of protein levels over two measurements of each sample, averaged over six L-form samples.

B. Cellular content of key muropeptide species indicates stable cell-wall composition throughout reversion. Integrated absorbance for each species is normalized to protein concentration for each measurement. To allow for comparison between muropeptide species, each curve has been normalized so that the abundance of each muropeptide species is 1 in exponentially growing, rod-shaped MG1655 cells.

C. Mole fractions of muropeptide species during reversion (solid coloured lines) as well as steady-state values for rod-shaped cells (dashed lines). Pentapeptides (M5, magenta) are enriched in L-forms and at early stages of reversion, but are absent from rod-shaped cells. Anhydromuropeptides (D44N, cyan) decrease over time, reflecting an increase in glycan strand length. Crosslinked species (dimer D44 and trimer T444) increase over time, consistent with recovery from cefsulodin treatment.

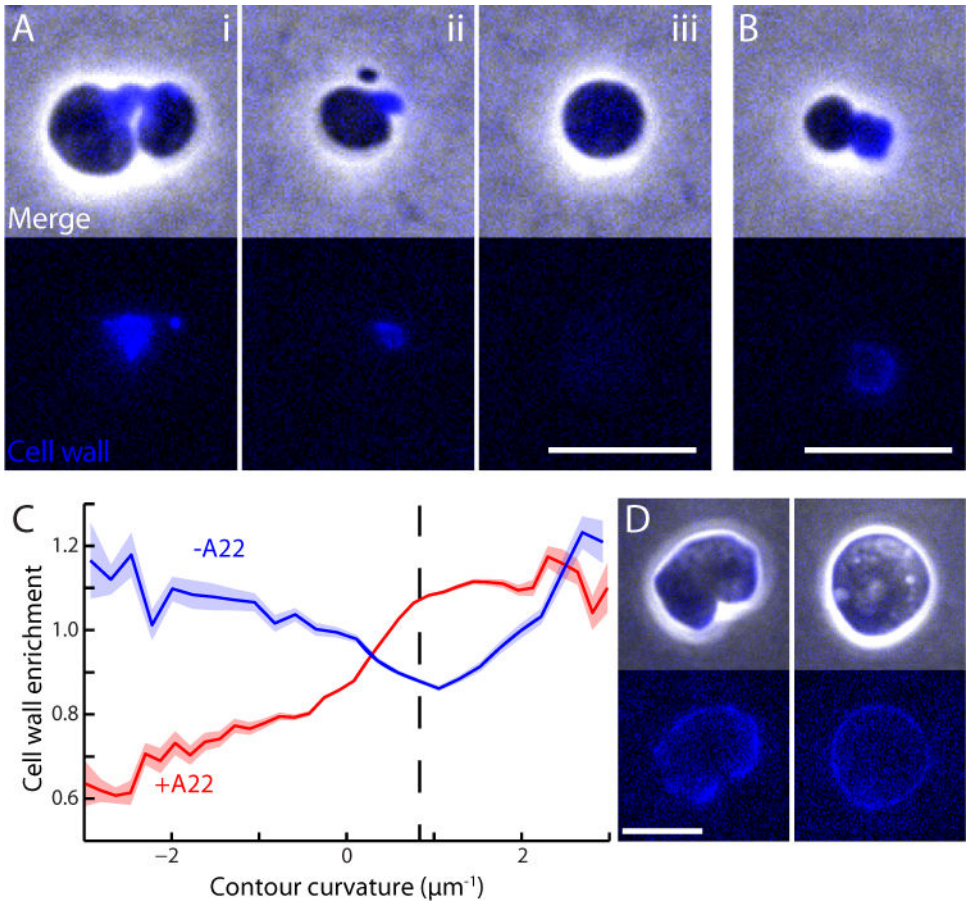

Fig. 4.

Subcellular localization of cell-wall material in propagating and reverting L-forms.

A, B, and D. Phase-contrast and epifluorescence images of FDAA staining of L-forms propagating (A), reverting (B), and reverting in the presence of A22 (D) in liquid culture reveals the subcellular distribution of cell-wall material. Scale bars: 5 μm.

A. In propagating L-forms, FDAA staining (and thus cell-wall material) localizes to septa (i) and old division sites (ii), but is not present in spherical cells (iii).

B. Cell-wall material in reverting L-forms is localized to non-spherical regions of the cell.

C. Mean cell-wall enrichment as a function of curvature. Blue curve: reverting L-forms (n = 375 cells). Red curve: reverting L-forms in the presence of A22 (n = 326 cells). Standard error of the mean is depicted in light blue and red curves. Reverting L-forms without A22 have minimum cell wall enrichment close to the curvature corresponding to spherical regions of the cell (dashed line), demonstrating that cell shape is a good proxy for the presence of cell-wall material. A22 treatment disrupts MreB polymers, and cells fail to target cell-wall material to regions of negative curvature.

D. Phase-contrast and epifluorescence images of FDAA staining of L-forms reverting in liquid culture in the presence of A22 (after 240 min). Despite the inability to regrow rod-like shapes, the cells still regrow a cell wall.

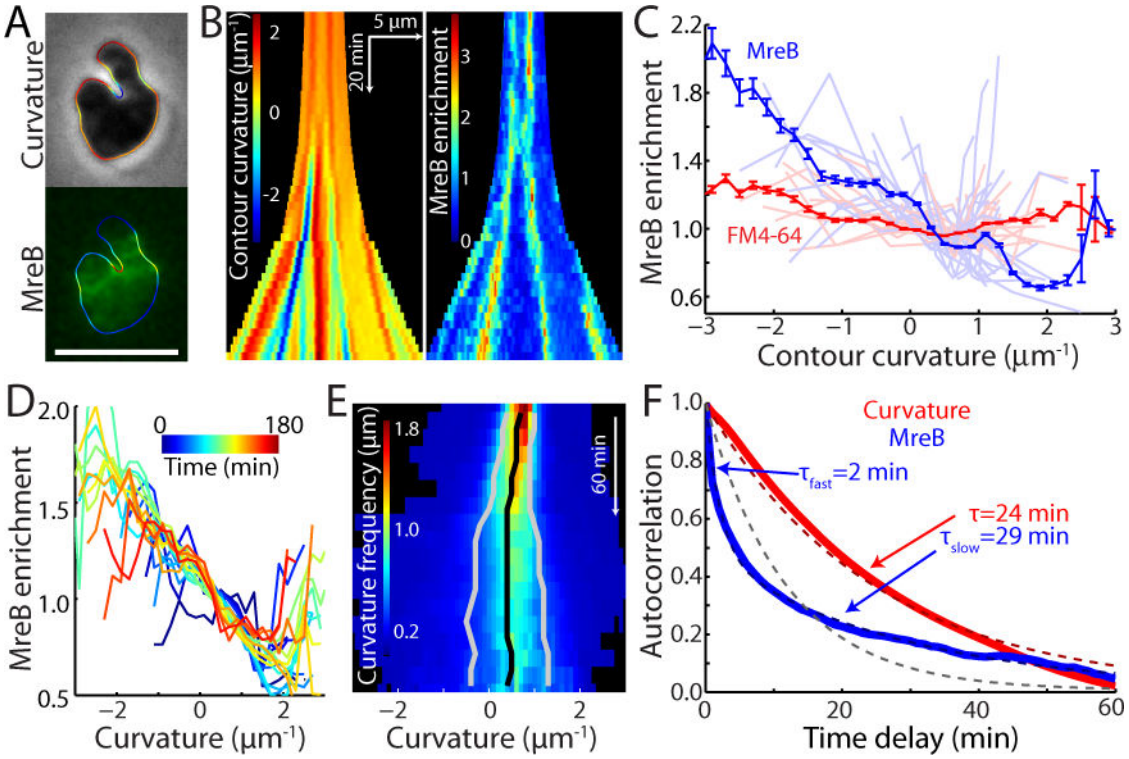

Fig. 5.

MreB localizes to regions of negative curvature in reverting L-forms.

A. Phase-contrast and epifluorescence images of reverting L-forms expressing a complementing MreB^{sw}-mVenus sandwich fusion. The outline of the phase image is coloured according to the local curvature of the outline, with invaginations defined to have negative curvature. The outline of the epifluorescence image is coloured according to the local MreB enrichment. MreB fluorescence is enhanced or depleted in regions of negative or positive curvature respectively. Scale bar: 5 μm.

B. Kymograph of the curvature and MreB fluorescence profiles over time for the reverting L-form cell in (A). The L-form is initially circular, with an approximately constant curvature profile; over time, it develops regions with negative curvature that associate with MreB fluorescence.

C. Enrichment of MreB in regions of negative curvature. Each light blue line represents an individual cell at a single time point, while the dark blue line represents the mean over time-lapse movies of n = 3 cells. The red lines show the enrichment signal of a membrane dye (FM4–64) for the same cells, demonstrating that the MreB enrichment is not due primarily to any three-dimensional deformations in the geometry of the cell. Error bars: standard error of the mean.

D. Curvature enrichment, sampled every 10 min after the first 25 min of reversion, rapidly converges to the average distribution in (C).

E. The kymograph of the distribution of curvatures across all cells broadens over time (black: mean; grey: mean ± standard deviations), indicating the adoption of increasingly non-spherical shapes, shows an increasing range of curvatures as time progresses. Data show means of n = 13 cells.

F. Autocorrelation functions of curvature (red) and MreB fluorescence (blue), averaged over the $n = 13$ cells in (D–E). The curvature autocorrelation is well fit by a single exponential (dark red, dashed line); the MreB autocorrelation is poorly fit by a single exponential (grey dotted line), but is well fit by the sum of two exponentials representing a fast and a slow timescale (dark blue, dashed line). Time constants τ indicate the time required to decay by a factor of e, the base of the natural logarithm.

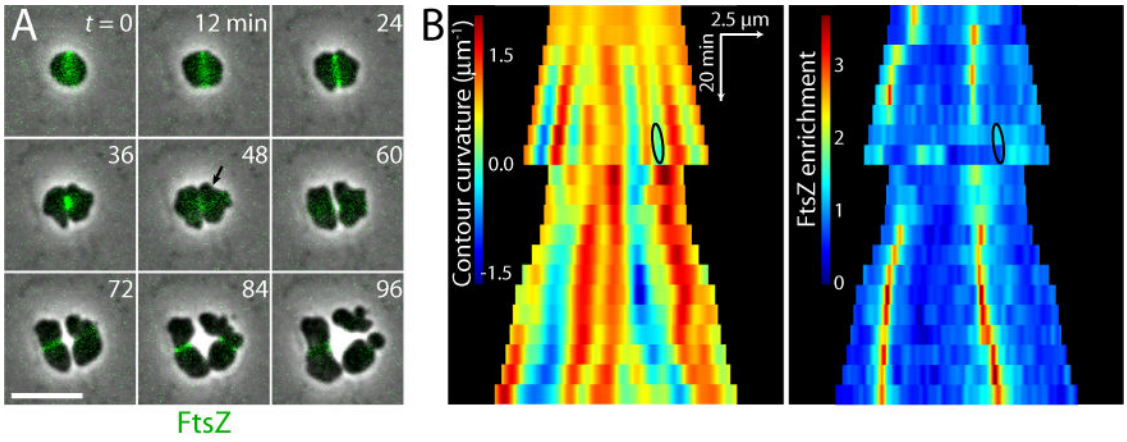

Fig. 6.

FtsZ forms rings during L-form reversion and initiates cell constriction.

A. Overlaid phase-contrast and epifluorescence time-course of a reverting L-form expressing a C-terminal FtsZ–GFP fusion (green). As is typical, FtsZ localizes in ring-like structures, the contraction of which is coordinated with division. Scale bar: 5 μm.

B. Kymograph of contour curvature (left) and FtsZ enrichment (right) for the cell in (A). FtsZ is mainly enriched at the division site rather than at regions of negative curvature, as demonstrated by the oval highlighting a region of negative curvature lacking FtsZ enrichment, indicated by the arrow in (A).